ACS OMEGA

http://pubs.acs.org/journal/acsodf

Article

Mechanistic Insights into the Dual Directing Group-Mediated C−H Functionalization/Annulation *via* a Hydroxyl Group-Assisted M^{III}-M^{V}-M^{III} Pathway

Huiying Xu,[#] Mengyao Bian,[#] Zhi Zhou, Hui Gao,* and Wei Yi*

Cite This: *ACS Omega* 2021, 6, 17642−17650

Read Online

ACCESS | Metrics & More | Article Recommendations | Supporting Information

ABSTRACT: The experimental investigations on the catalyst [$Cp^*Rh(OAc)_2$ and $Cp^*Ir(OAc)_2$)]-controlled [3 + 2] and [4 + 2] annulations of oximes with propargyl alcohols have been finished in our previous work and a supposed dual directing group-mediated reaction pathway has been deduced for the chemo-divergent product synthesis. However, the detailed interaction modes of the dual directing groups binding with the corresponding metal center to achieve the above observed chemoselectivity remain unclear and even contradict. For instance, the calculational traditional dual direct coupling transition states suggested that both $Cp^*Rh(OAc)_2$- and $Cp^*Ir(OAc)_2$-catalyzed reactions would generate five-membered indenamines as the dominant products *via* [3 + 2] annulation. To address this concern, herein, systematic DFT calculations combined with proof-of-concept experiments have been carried out. Accordingly, a novel and more favorable M^{III}-M^{V}-M^{III} reaction mechanism, which involves an unprecedented HOAc together with a hydroxyl group-assisted reaction pathway in which the hydroxyl group acts as double effectors for the formation of M−O coordination and [MeO···H···O(CCH_3)O···H···O] bonding interactions, was deduced. Taken together, the present results would provide a rational basis for future development of the dual directing group-mediated C−H activation reactions.

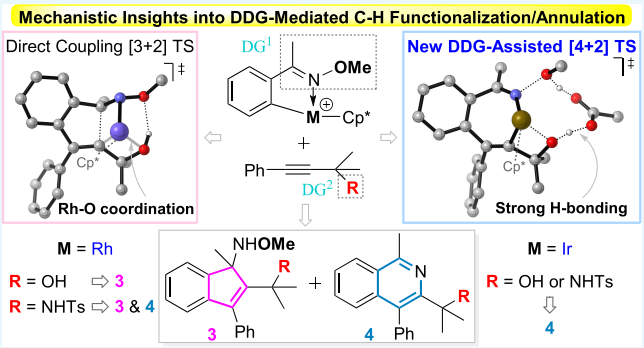

1. INTRODUCTION

In recent years, C−H activation/annulation enabled by transition metal (TM) catalysts has received significant attention in the synthetic chemistry community, especially for heterocyclic framework construction.[1,2] Undoubtedly, direct C−H functionalization has represented a versatile strategy for transformation of easily available and unactivated substrates in an atom-economic fashion.[3] Compared to the single directing group-assisted strategy, the dual directing group (DDG) strategy would bring in a richer variety and thus give more complicated products with excellent control of the selectivity. Among those, the development of the hydroxyl group as a master directing partner of the DDGs has been preliminarily established and is successful in the field of TM-catalyzed C−H activation under the efforts of many scientific researchers.[4] In general, when the coupling partners are installed with the hydroxyl group, e.g., the representative propargyl alcohol framework,[5] the binding affinity potential of the hydroxyl group with the TM catalyst shows unique advantages in both controlling the site-/regioselectivity and improving the reactivity.

Following the pioneering work of TM-catalyzed C−H activation reactions with propargyl alcohols, up to date, TM (including ruthenium, rhodium, and iridium)-catalyzed C−H activations of oximes,[6] amides,[7] arylamines,[8] and other substrates[9] have been developed, which provided abundant references for the synthesis of various privileged structural motifs. In 2018, we have also shown that the chemodivergent reaction pathways for the direct synthesis of indenamine and isoquinoline skeletons could be switched by tuning the TM catalyst species *via* controllable [3 + 2] and [4 + 2] annulations (Scheme 1).[10] The experimental studies revealed that the hydroxyl group in the tertiary propargyl alcohol substrate plays a decisive role in determining the outcome of the reaction with tunable chemoselectivity. Based on these advances, we reasoned that the different binding affinity and coordination environment of the hydroxyl group with the Rh and Ir metal centers might enable distinct annulation modes. Nevertheless, a more detailed reaction[11] mechanism is still unclear and thus it should be systematically expounded, since such a DDG-assisted strategy has emerged as a straightforward and powerful

Received: April 25, 2021
Accepted: June 18, 2021
Published: July 1, 2021

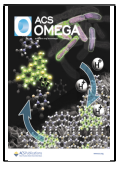

https://doi.org/10.1021/acsomega.1c02183
ACS Omega 2021, 6, 17642−17650

Scheme 1. Previously Reported Reactions of Catalyst-Controlled [4 + 2] and [3 + 2] Annulations

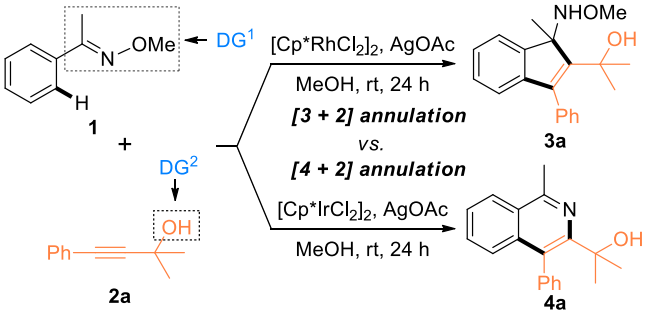

method for the target compound synthesis in current C−H activation reactions. Considering the significance of the DDG-assisted C−H functionalization and based on the previous density functional theory (DFT) calculations for TM-catalyzed C−H activation/annulation reactions,[12,13] herein, systematic DFT calculations and the designed proof-of-concept experimental study have been accordingly carried out by using the catalytic coupling of oximes and propargyl alcohols as the effectors, which give detailed insight into the DDG-enabled mechanism, and thus, it also provides some key inspiration on how to achieve the high chemoselectivity in the future C−H functionalization reactions.

2. RESULTS AND DISCUSSION

2.1. Traditional [3 + 2] and [4 + 2] Annulation Pathways. Based on our experimental observation[10] and previous literature precedents[14] on TM-catalyzed C−H activation/annulation with alkynes, DFT calculations were utilized to probe the reaction mechanism using the five-membered rhodacycle and iridacycle intermediates (^{M}**INT-0**) as the starting point, respectively. It is noted that from the previous theoretical study by Xia *et al.*,[12i] the formation of Cp*Rh(OAc)$_2$ from [Cp*RhCl$_2$]$_2$ and CsOAc is favorable in energetics. Similar to the geometry of Cp*Rh(OAc)$_2$ reported in their work, the coordinating complex between ^{M}**INT-0** and the OAc anion (^{M}**INT-0′**) or the substrate **2a** (^{M}**INT-0″**) was found to hold the same binding mode in which the Rh or Ir center has three coordination sites occupied as well as the η^5 coordination of the Cp* ligand (Figure 1). Also, calculations indicate that the transformation process between these three intermediates is feasible. Figure 1 shows that the activation barriers of the alkyne insertion step are 17.1 and 20.1 kcal/mol (from ^{M}**INT-0′** to ^{M}**TS-0**) in the Rh- and Ir-catalyzed reaction systems, respectively. Therefore, the alkyne insertion process from ^{M}**INT-0′** is a feasible process, both kinetically and thermodynamically favorable. Following the alkyne insertion step, the seven-membered intermediates ^{Rh}**INT-1** and ^{Ir}**INT-1** (Figure 2) are obtained through the M-C^2 bonding (2.04 and 2.05 Å, respectively) and the M-N^1 (2.14 and 2.11 Å, respectively) and M-O^2 (2.24 Å for both) coordination interactions between the catalyst and the substrate. On the other hand, the alternative regioselective transition state ^{M}**TS-0$_i$** was assessed and ruled out since its energy barrier is higher than ^{M}**TS-0** by 1.8−3.2 kcal/mol.

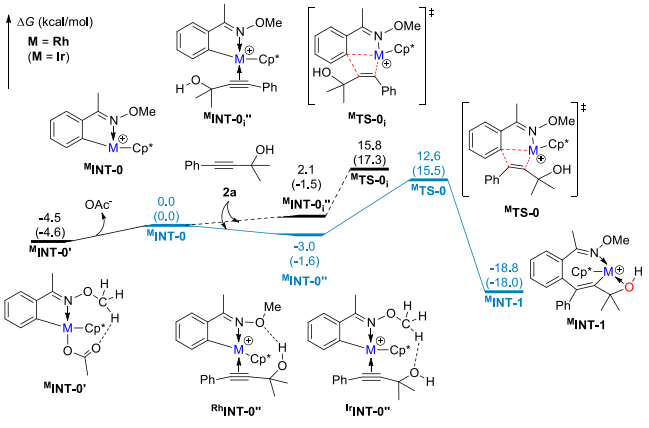

Figure 1. Potential energy profiles of the alkyne insertion process (M = Rh or Ir).

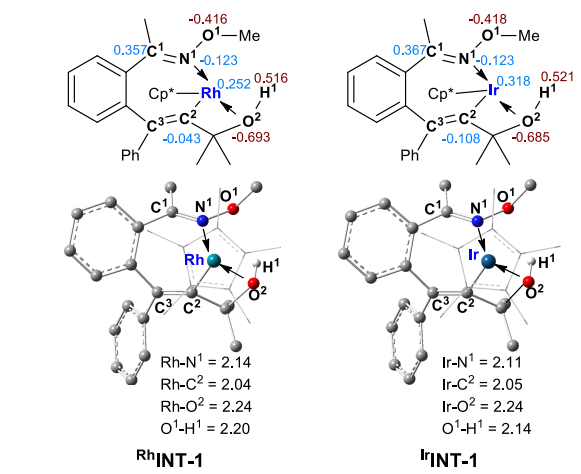

Figure 2. Important geometry parameters (in Å) and NBO charge distributions of ^{Rh}**INT-1** and ^{Ir}**INT-1**.

Subsequently, in the Rh-catalyzed reaction, direct C−C bond formation and C−N bond formation pathways (paths a and b in Figure 3) from the seven-membered rhodacycle intermediate ^{Rh}**INT-1** are accessed and the lower energy of ^{Rh}**TS-1a** (see Figure S1 in the Supporting Information for more geometry parameters) suggests that the [3 + 2]

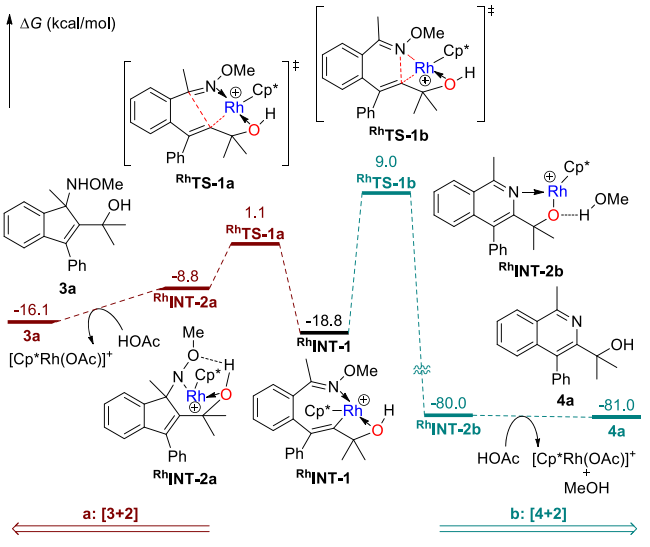

Figure 3. Potential energy profile of the direct C−C coupling and C−N coupling pathways with the Rh catalyst.

https://doi.org/10.1021/acsomega.1c02183
ACS Omega 2021, 6, 17642−17650

annulation ($\Delta G^{\neq}$ = 19.9 kcal/mol) to yield the indenamine product **3a** is prior to the [4 + 2] annulation ($\Delta G^{\neq}$ = 27.8 kcal/mol) to provide the isoquinoline product **4a**. This is in agreement with the experimental observation (Scheme 1). However, in the case of the Ir catalyst, the calculation on the two direct coupling pathways (Figure 4) reveals that the [3 + 2] annulation ($\Delta G^{\neq}$ = 26.6 kcal/mol) *via* ^{Ir}**TS-1a** is also more favorable than the [4 + 2] annulation ($\Delta G^{\neq}$ = 33.0 kcal/mol) *via* ^{Ir}**TS-1b**. Therefore, such results give a clear contradiction with the corresponding experimental results (Scheme 1). By reviewing the computational data, we noted that the C−N bond formation pathway is characterized as a concerted and asynchronous process in which C−N reductive elimination is followed by a barrierless N−O bond cleavage with the formation of methanol (Figure S2). Notably, an unstable M^{I} intermediate on the optimization profile of ^{Ir}**INT-2b** is observed for the M^{III}-M^{I}-M^{III} reaction pathway hypothesis. Inspired by the conflict between the above theoretical calculations and experimental results, in-depth studies have been implemented with the aim to uncover the detailed reaction process patterns and to define the refined interaction modes in some critical transition states.

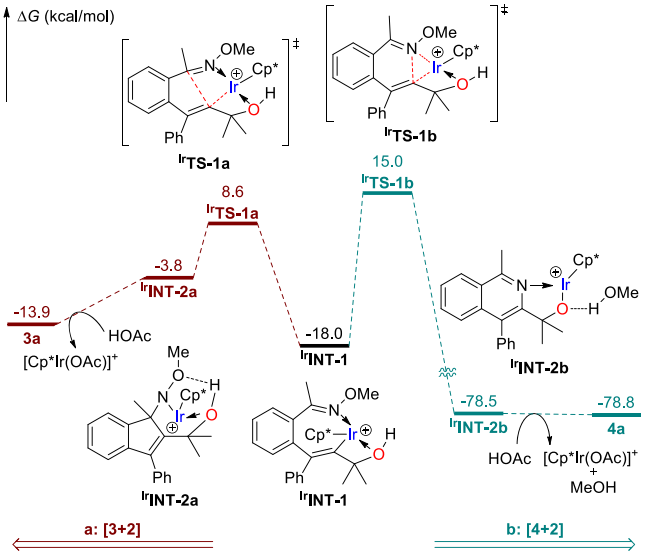

Figure 4. Potential energy profile of the direct C−C coupling and C−N coupling pathways with the Ir catalyst.

2.2. Identifying the Binding Mode of the DDGs. When close examining the binding modes of DDGs with the catalyst, the isomer forms of the transition state ^{Rh}**TS-1a** were located. As shown in Figure 5, ^{Rh}**TS-1a** presents an attractive [MeO···H] bonding (1.98 Å) and a classical DDG-assisted Rh−O coordination (2.27 Å),[4b,15] thus giving a relatively low free energy (ΔG = 1.1 kcal/mol). In the traditional DDG-assisted and DG-mediated transition states (^{Rh}**TS-1a**$_{iso1}$ and ^{Rh}**TS-1a**$_{iso2}$, respectively), higher free energy (1.1 kcal/mol *vs* 3.1 and 7.2 kcal/mol) is involved due to the absence of the [MeO···H] bonding and/or the Rh−O coordination. Taken together, these results suggested that the existence of the [MeO···H] bonding interaction plays a key role in the DDG-assisted C−H activation reaction. To the best of our knowledge, this is the first time that such an innovative role of the DDGs is being disclosed.

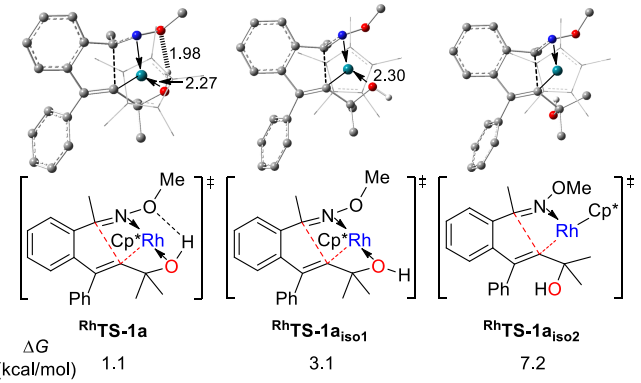

Figure 5. Coordination modes of DDG with the Rh catalyst in the C−C coupling transition states.

2.3. Hydroxyl Group-Assisted M^{III}-M^{V}-M^{III} Mechanism of the [4 + 2] Annulation Reaction. With the innovative interaction mode of the DDGs binding to the catalyst in hand, further calculations are carried out to elucidate a new and alternative reaction pathway to replace the traditional annulation mechanism shown in Figures 3 and 4. Thus, the novel hydrogen-bonding interaction, metal-O coordination, and other noncovalent bonds contributed by the DDGs for stabilizing reaction transition states and intermediates are reconsidered and further optimized. In addition, the methanol formation process in path b also arouses our concern.

After many attempts, a reasonable [4 + 2] annulation mechanism involving the hydrogen-bonding interactions and the high-valent metal intermediate formation has been obtained (Figure 6). As demonstrated in Figure 6, the overall barrier of the Cp*Ir(OAc)$_2$-catalyzed annulation *via* the H-bonding-assisted [4 + 2] transition state ^{Ir}**TS-1c** ($\Delta G^{\neq}$ = 22.1 kcal/mol) is obviously lower than those of the direct C−C and C−N coupling pathways (26.6 and 33.0 kcal/mol, respectively). Moreover, from the point of view of the stepwise C−N coupling stage, the seven-membered iridacycle intermediate ^{Ir}**INT-1** undergoes N−O bond oxidative cleavage *via* ^{Ir}**TS-1c**, followed by the extrusion of methanol to provide the Ir(V) intermediate ^{Ir}**INT-2c**. Finally, the C−N reductive elimination *via* ^{Ir}**TS-2c** gives the [4 + 2] annulation isoquinoline product **4a**. Considering the reasonable free energy barriers in all stages, this newly proposed C−N coupling mechanism *via* the

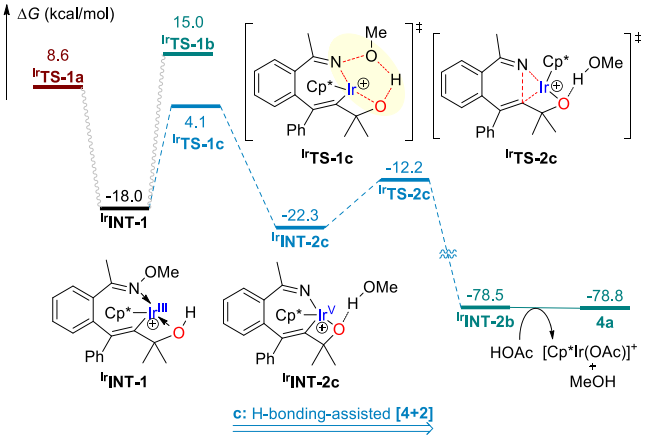

Figure 6. Potential energy profile of the hydrogen-bonding-assisted C−N coupling pathway with the Ir catalyst.

https://doi.org/10.1021/acsomega.1c02183
ACS Omega 2021, 6, 17642−17650

Ir^{III}-Ir^{V}-Ir^{III} reaction pathway that involves an unprecedented hydrogen-bonding interaction can be defined as an innovative mechanistic basis for the DDG-induced C−H activation reaction mode proposal.

On the other hand, if we look closely at the geometries of the seven-membered iridacycle intermediates and transition states in the three pathways with the Cp*Ir(OAc)$_2$ catalyst (Figures 2 and 7 and Figure S1), it can be found that the

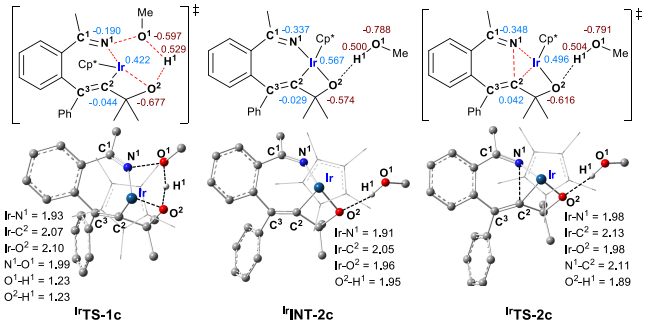

Figure 7. Important geometry parameters (in Å) and NBO charge distributions of ^{Ir}**TS-1c**, ^{Ir}**INT-2c**, and ^{Ir}**TS-2c**.

formation of the hydrogen-bonding interaction is very critical for the main product formation. In the intermediate ^{Ir}**INT-1**, the distance between the O^1 atom and the H^1 atom is larger than 2.0 Å (2.14 Å), indicating that there is a weak hydrogen-bonding interaction. For the concerted C−C bond and C−N bond formation transition states ^{Ir}**TS-1a** and ^{Ir}**TS-1b**, the distances of the O^1−H^1 bonds are slightly shortened (1.87 and 2.03 Å). Meanwhile, the length of the O^1−H^1 bond is much shorter (1.23 Å) in the transition state ^{Ir}**TS-1c**. Obviously, the disclosed hydrogen-bonding-involved binding mode gives a reasonable explanation for the conflict between experimental results and calculation results of the traditional coupling reaction mechanism for the Cp*Ir(OAc)$_2$-catalyzed reaction.

However, whether the new mechanism holds for the case in which the [3 + 2] annulation product under the Cp*Rh(OAc)$_2$ catalysis was observed as the major product remains unclear and needs to be answered. To solve this question, the stepwise C−N coupling pathway has been calculated by employing Cp*Rh(OAc)$_2$ as the catalyst based on the newly proposed hydrogen-bonding-assisted mechanism. As demonstrated in Figure 8, it shows that the activation barrier of the [3 + 2] cyclization transition state ^{Rh}**TS-1a** ($\Delta G^{\neq}$ = 19.9 kcal/mol) containing the [MeO···H] bonding interaction is much lower than that of [4 + 2] annulation *via* ^{Rh}**TS-1b** and ^{Rh}**TS-1c** by 7.9 and 7.6 kcal/mol, respectively. This means that the pathway toward the C−C bond formation product **3a** is more favorable, which is also consistent with the related experimental data.

To further examine the electronic effect in the DDG-assisted C−H functionalization reaction, the natural bond orbital (NBO) charge population of the important intermediates and transition states has been also calculated. As listed in Figures 2 and 7 and Figure S1, the NBO charges on the Rh atom are 0.252, 0.291, 0.251, and 0.298 in ^{Rh}**INT-1**, ^{Rh}**TS-1a**, ^{Rh}**TS-1b**, and ^{Rh}**TS-1c**, respectively. The small differences among these values cannot guarantee that the pathway *via* ^{Rh}**TS-1c** can perfectly compete with the other two pathways. However, the NBO charges on the Ir atom are 0.318, 0.363, 0.321, and 0.422 in ^{Ir}**INT-1**, ^{Ir}**TS-1a**, ^{Ir}**TS-1b**, and ^{Ir}**TS-1c**, respectively. These

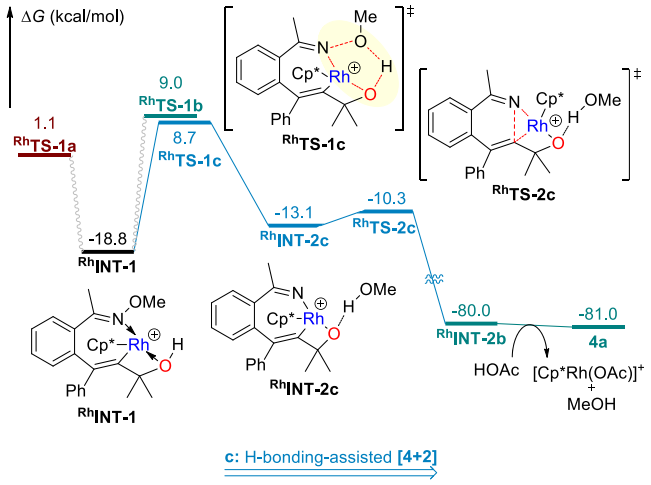

Figure 8. Potential energy profile of the hydrogen-bonding-assisted C−N coupling pathway with the Rh catalyst.

results show that the Ir metal center gains much more positive charge in ^{Ir}**TS-1c** than ^{Ir}**TS-1a** and ^{Ir}**TS-1b**, which can significantly stabilize the hydrogen-bonding-assisted C−N coupling transition state ^{Ir}**TS-1c**, thus making the [4 + 2] annulation more facile.

2.4. HOAc and Hydroxyl Group-Assisted Annulation Mechanism: Inner- and Outer-Sphere Hydrogen Bonding. Since the hydrogen bonding plays a critical role in the reaction involving a hydroxyl group as a DG, the solvent MeOH and the HOAc molecules formed in the C−H/N−H activation steps may possibly take part in the interaction of the hydrogen-bonding network. Therefore, based on previous investigations on the inner- or outer-sphere hydrogen bonding reported by us and other literature,[12i,16] the three pathways of Ir-catalyzed annulation assisted by MeOH or HOAc were calculated, respectively. It can be seen that the involvement of one methanol molecule might increase the free energies of the seven-membered iridacycle and the three transition states by more than 3 kcal/mol (Figure S3). It means that the solvent molecule is not likely involved in the hydrogen-bonding network initiated by the DDG.

However, it is different in the HOAc case (Figure 9). The involvement of HOAc is still not good for facilitating the traditional [3 + 2] and [4 + 2] pathways, paths a1 and b1. Meanwhile, the relative free energy of the H-bonding-assisted [4 + 2] transition state ^{Ir}**TS-1c$_A$** in path c1 is −0.4 kcal/mol and its activation barrier is 17.6 kcal/mol (*vs* 22.1 kcal/mol for ^{Ir}**TS-1c**). In the geometry of ^{Ir}**TS-1c$_A$** (Figure 10), the hydrogen atom of the hydroxyl group transfers to the acetate-O, while the hydrogen atom of HOAc transfers to the oxygen atom of OMe, which facilitates the cleavage of the N−O bond. The H-bonds are nearly linear in the HOAc-assisted transition state ^{Ir}**TS-1c$_A$** (168° and 167°). Compared with the NBO charge of Ir (0.422) for ^{Ir}**TS-1c** (Figure 7), the NBO charge of Ir is more positive (0.443) for ^{Ir}**TS-1c$_A$** (Figure 10), which indicates that acetic acid could enhance the oxidative N−O bond dissociation process. Furthermore, the addition of one more HOAc molecule may not be favored (^{Ir}**TS-1c$_{2A}$**, ΔG = 2.5 kcal/mol). Also, when the hydroxyl group of the substrate does not join the hydrogen-bonding network, it may not enable the [4 + 2] annulation *via* ^{Ir}**TS-1c$_{Aiso}$** because of the high energy barrier of 36.8 kcal/mol. That is to say, the DDG effect is likely to be one of the critical

https://doi.org/10.1021/acsomega.1c02183
ACS Omega 2021, 6, 17642−17650

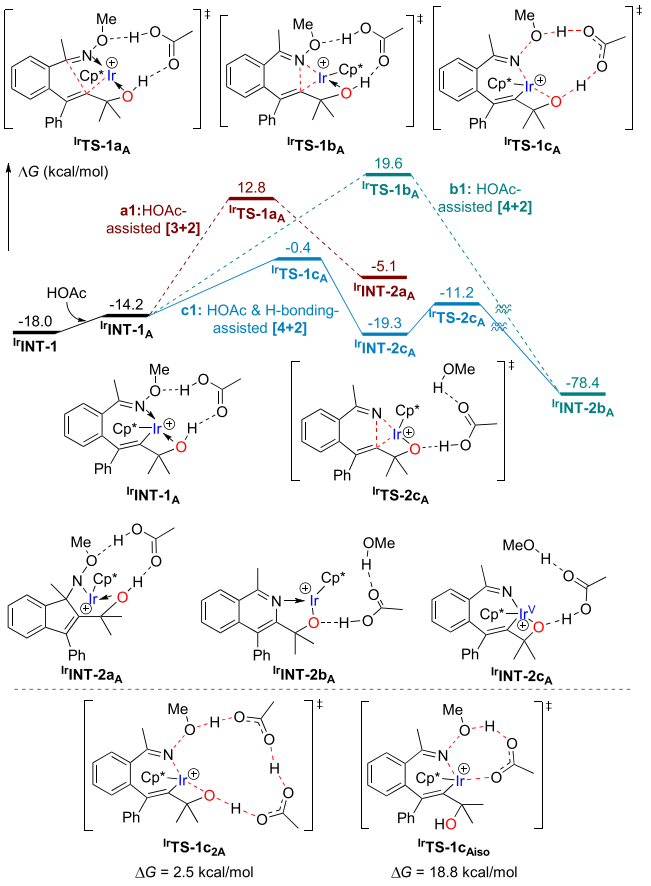

Figure 9. Potential energy profiles of the HOAc and hydrogen-bonding-assisted annulation pathway with the Ir catalyst.

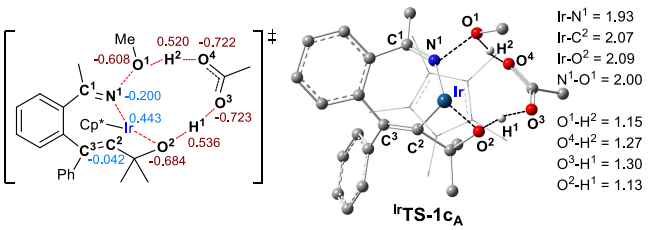

Figure 10. Important geometry parameters (in Å) and NBO charge distribution of ^{Ir}**TS-1c$_A$**.

chemoselectivity-controlling factors in these types of reactions. These results indicate that the electrostatic interaction in the reaction center can significantly affect the reaction energy barrier and even change the chemoselectivity. In fact, in our experiment, Ag^+ or Cu^{2+} cations could possibly act as a Lewis acid in the [3 + 2] annulation by coordinating with the nitrogen atom of the directing group(s), which may accelerate the reaction.

2.5. Experimental Proof of Concept. From the discussion on the three abovementioned reaction mechanisms of the C−H functionalization/annulation, the switchable chemoselectivity by the metal catalyst is well understood. To further confirm the compatibility of the newly proposed hydrogen-bonding-assisted M^{III}-M^{V}-M^{III} mechanism, we designed iridium- and rhodium-catalyzed C−H activation/annulation reaction systems using *O*-methyl oxime and 4-methyl-*N*-(2-methyl-4-phenylbut-3-yn-2-yl)benzene-sulfonamide (**2b**) as the model substrates for the proof of concept (Scheme 2). The results from DFT calculations (Figure S4) demonstrate that when the hydroxyl group (−OH) is replaced

Scheme 2. Newly Designed Rh- and Ir-Catalyzed Annulation Reactions

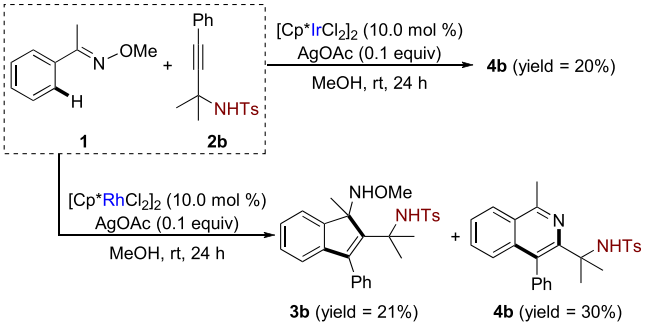

by the *p*-toluenesulfonamide moiety (−NHTs) in the alkyne substrate, the reaction of the seven-membered iridacycle intermediate ^{Ir}**INT-1$_N$** may take place in the HOAc and H-bonding-assisted [4 + 2] pathway (path c1) *via* ^{Ir}**TS-1c$_{NA}$** (ΔG = −6.9 kcal/mol) with a relatively low overall free energy barrier (ΔG = 4.1 kcal/mol for ^{Ir}**TS-1a$_N$**, 13.5 kcal/mol for ^{Ir}**TS-1b$_N$**, and 0.2 kcal/mol for ^{Ir}**TS-1c$_N$**, respectively) to provide the dominant product **4b**. These computational results are verified by the subsequent experiments (Scheme 2, see the Supporting Information for more experimental details) in which only isoquinoline product **4b** was observed. However, it is found that in the Rh-catalyzed reaction, path c has a significantly higher energy barrier than the [3 + 2] pathway (path a), while path c1 has a competitive barrier with path a (Figure 11). The free energy difference between ^{Rh}**TS-1a$_N$** (ΔG = −1.4 kcal/mol) and ^{Rh}**TS-1c$_{NA}$** (ΔG = −0.5 kcal/mol) is only 0.9 kcal/mol, which means that both of these two pathways may take place at the same time. These calculational results are in agreement with the experimental observations that Rh-catalyzed annulation of **2b** gave both [3 + 2] and [4 + 2] products (Scheme 2). These suggest that the DDG effect may enable the [4 + 2] annulation even in the Rh-catalyzed case.

The designed experimental result gives a clear proof-of-concept verification for the abovementioned HOAc and hydroxyl group-assisted M^{III}-M^{V}-M^{III} mechanism *via* hydrogen bonding. Moreover, it reveals that the *p*-toluenesulfonamide group (−NHTs) can also be utilized as an alternative directing group in the relevant DDG-assisted TM-catalyzed C−H functionalization/annulation since it has similar interaction features with the OH group and exhibits special properties under certain conditions.

On the other hand, to further illustrate the role of the hydroxyl group in the [4 + 2] annulation for isoquinoline products, the calculations on paths b and c1$_{iso}$ of **2c** (PhCC^{t}Bu)[10] (see Figure S5 and Table S1 in the Supporting Information) have been done for comparison with **2a**. As discussed earlier, hydrogen-bonding interactions have little effect on the energy barrier for the Rh-catalyzed reaction of **2a**. Meanwhile, hydrogen bonding plays a crucial role in the Ir-catalyzed reaction of **2a**. For the substrate **2c**, the energy barriers of path b catalyzed by Rh and Ir are 0.4 and 2.3 kcal/mol higher than that of **2a**, respectively. Also, for **2c**, paths c and c1 do not exist and path c1$_{iso}$ catalyzed by Rh and Ir has a barrier higher than 30 kcal/mol. These results indicate one of

https://doi.org/10.1021/acsomega.1c02183
ACS Omega 2021, 6, 17642−17650

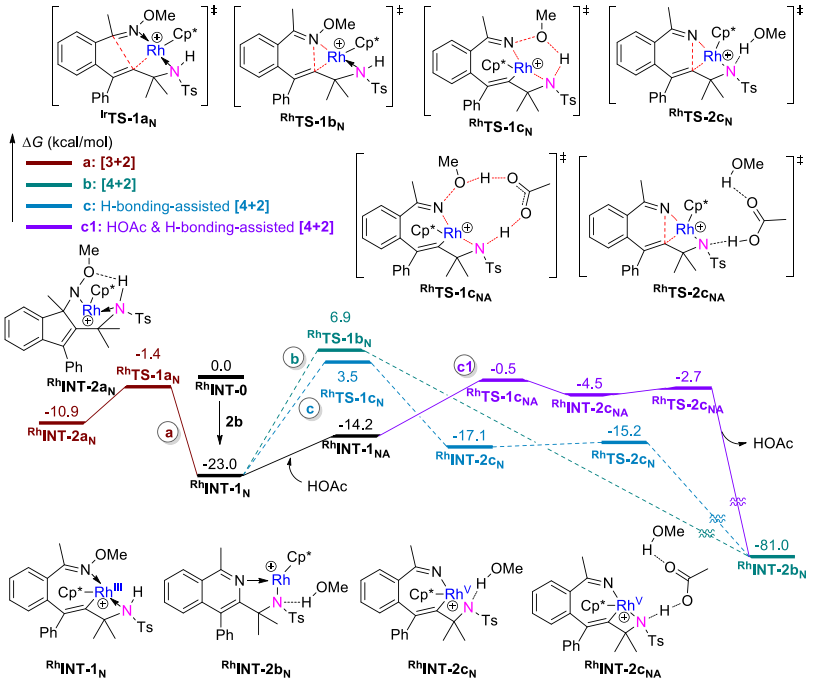

Figure 11. Potential energy profiles of the three annulation pathways with the Rh catalyst when the −OH group is replaced by −NHTs.

the reasons why [4 + 2] annulation may occur with the Rh catalyst, while [4 + 2] annulation cannot occur with the Ir catalyst. This again reveals the importance of DDG in the involved TM-catalyzed [4 + 2] annulation.

3. CONCLUSIONS

Through the computational and experimental studies of the [3 + 2] and [4 + 2] annulations of oximes with propargyl alcohols catalyzed by $Cp^*Rh(OAc)_2$ and $Cp^*Ir(OAc)_2$, we proposed a novel hydroxyl group-mediated [4 + 2] annulation mechanism that involves the multiple interactions between dual directing groups and the metal center. DFT calculations suggest a new type of hydrogen-bonding-assisted M^{III}-M^{V}-M^{III} mechanism for the HOAc and hydroxyl group-assisted [4 + 2] annulation process. Taken together, these results not only give a clear explanation for the chemoselectivity but also provide a rational basis for future development of the dual directing group-mediated C−H activation reactions. Further experimental design and development based on the disclosed key hydrogen-bonding-assisted M^{III}-M^{V}-M^{III} mechanism are ongoing in our laboratory.

4. METHODS

4.1. Computational Details. All of the DFT calculations were performed with the Gaussian 09 quantum chemical package.[17] The B3LYP[18] functional with the standard 6-31G(d) basis set (Lanl2dz[19] basis set for Rh and Ir) (BS1) was used for geometry optimizations. The vibrational frequencies were computed at the same level of theory to confirm whether each optimized structure is an energy minimum or a transition state and to evaluate its zero-point vibrational energy (ZPVE). Intrinsic reaction coordinate (IRC) calculations[20] were carried out to confirm that all transition state structures connect the corresponding reactants and products. Solvent effects in methanol were estimated by using the SMD[21] solvation method at the B3LYP level of theory with the DFT-D3 dispersion corrections.[22] Herein, the Stuttgart/Dresden effective core potential (SDD)[23] was used for Rh and Ir and the 6-311++G(d,p) basis set was used for all other atoms (BS2). Unless otherwise specified, relative free energies of all reported structures were calculated under standard conditions (101,325 Pa and 298.15 K). Cartesian coordinates and total energies of all reported structures are given in the Supporting Information.

4.2. Experimental Methods. The mixture of (*E*)-1-phenylethan-1-one-*O*-methyl oxime (**1**) (0.2 mmol, 1.0 equiv), 4-methyl-*N*-(2-methyl-4-phenylbut-3-yn-2-yl)-benzenesulfonamide (**2b**) (0.2 mmol, 1.0 equiv), $[Cp^*RhCl_2]_2$ (10.0 mol %), and AgOAc (0.1 equiv) in MeOH (2.0 mL) was stirred in a sealed tube at room temperature for 24 h without exclusion of air or moisture. Afterward, the mixture was diluted with EA, transferred to a round-bottom flask, and concentrated. The crude product was purified by preparative TLC (eluent: PE/EA = 5/1) to afford the desired products **3b** and **4b**. The mixture of **1** (0.2 mmol, 1.0 equiv), **2b** (0.2 mmol, 1.0 equiv), $[Cp^*IrCl_2]_2$ (10.0 mol %), and AgOAc (0.1 equiv) in MeOH (2.0 mL) was stirred in a sealed tube at room temperature for 24 h without exclusion of air or moisture. Afterward, the mixture was diluted with EA, transferred to a round-bottom flask, and concentrated. The crude product was purified by preparative TLC (eluent: PE/EA = 5/1) to afford the desired product **4b**. Detailed experimental information and characterization data are given in the Supporting Information.

■ ASSOCIATED CONTENT

Supporting Information

The Supporting Information is available free of charge at https://pubs.acs.org/doi/10.1021/acsomega.1c02183.

Additional computational results and Cartesian coordinates, energies, and imaginary frequencies of all stationary points; detailed experimental procedure, characterization data, and copies of ^1H and ^{13}C spectra (PDF)

https://doi.org/10.1021/acsomega.1c02183
ACS Omega 2021, 6, 17642−17650

AUTHOR INFORMATION

Corresponding Authors

Hui Gao − *Guangzhou Municipal and Guangdong Provincial Key Laboratory of Protein Modification and Degradation & Molecular Target and Clinical Pharmacology, State Key Laboratory of Respiratory Disease, School of Pharmaceutical Sciences, Guangzhou Medical University, Guangzhou 511436, China;* orcid.org/0000-0002-8736-4485; Email: gaoh9@gzhmu.edu.cn

Wei Yi − *Guangzhou Municipal and Guangdong Provincial Key Laboratory of Protein Modification and Degradation & Molecular Target and Clinical Pharmacology, State Key Laboratory of Respiratory Disease, School of Pharmaceutical Sciences, Guangzhou Medical University, Guangzhou 511436, China;* orcid.org/0000-0001-7936-9326; Email: yiwei@gzhmu.edu.cn

Authors

Huiying Xu − *Guangzhou Municipal and Guangdong Provincial Key Laboratory of Protein Modification and Degradation & Molecular Target and Clinical Pharmacology, State Key Laboratory of Respiratory Disease, School of Pharmaceutical Sciences, Guangzhou Medical University, Guangzhou 511436, China;* orcid.org/0000-0001-9025-4183

Mengyao Bian − *Guangzhou Municipal and Guangdong Provincial Key Laboratory of Protein Modification and Degradation & Molecular Target and Clinical Pharmacology, State Key Laboratory of Respiratory Disease, School of Pharmaceutical Sciences, Guangzhou Medical University, Guangzhou 511436, China*

Zhi Zhou − *Guangzhou Municipal and Guangdong Provincial Key Laboratory of Protein Modification and Degradation & Molecular Target and Clinical Pharmacology, State Key Laboratory of Respiratory Disease, School of Pharmaceutical Sciences, Guangzhou Medical University, Guangzhou 511436, China;* orcid.org/0000-0002-6521-8946

Complete contact information is available at: https://pubs.acs.org/10.1021/acsomega.1c02183

Author Contributions

#H.X. and M.B. contributed equally to this work.

Notes

The authors declare no competing financial interest.

ACKNOWLEDGMENTS

We acknowledge financial support from the National Natural Science Foundation of China (81502909 and 21603279), China Postdoctoral Science Foundation (2019M662854), and Guangdong Natural Science Funds for Distinguished Young Scholar (2017A030306031).

REFERENCES

(1) (a) Song, L.; Van der Eycken, E. V. Transition Metal-Catalyzed Intermolecular Cascade C−H Activation/Annulation Processes for the Synthesis of Polycycles. *Chem. − Eur. J.* **2021**, *27*, 121−144. (b) Achar, T. K.; Maiti, S.; Jana, S.; Maiti, D. Transition Metal Catalyzed Enantioselective C(sp^2)−H Bond Functionalization. *ACS Catal.* **2020**, *10*, 13748−13793. (c) Lam, N. Y. S.; Wu, K.; Yu, J.-Q. Advancing the logic of chemical synthesis: C−H activation as strategic and tactical disconnections for C−C bond construction. *Angew. Chem., Int. Ed.* **2021**, DOI: 10.1002/anie.202011901. (d) Piou, T.; Rovis, T. Electronic and Steric Tuning of a Prototypical Piano Stool Complex: Rh(III) Catalysis for C-H Functionalization. *Acc. Chem. Res.* **2018**, *51*, 170−180. (e) Zhu, Y.; Zhao, X.; Wu, Q.; Chen, Y.; Zhao, J. Research Advances in C—H Bond Activation of Multitasking *N*-Phenoxyamides. *Acta Phys. − Chim. Sin.* **2019**, *35*, 989−1004. (f) Jiang, X.; Hao, J.; Zhou, G.; Hou, C.; Hu, F. Recent Advances in *N*-Phenoxyacetamides Directed C—H Bond Functionalization. *Chin. J. Org. Chem.* **2019**, *39*, 1811−1830.

(2) (a) Gensch, T.; Hopkinson, M. N.; Glorius, F.; Wencel-Delord, J. Mild metal-catalyzed C−H activation: examples and concepts. *Chem. Soc. Rev.* **2016**, *45*, 2900−2936. (b) Shin, K.; Kim, H.; Chang, S. Transition-Metal-Catalyzed C−N Bond Forming Reactions Using Organic Azides as the Nitrogen Source: A Journey for the Mild and Versatile C−H Amination. *Acc. Chem. Res.* **2015**, *48*, 1040−1052. (c) Jiao, J.; Murakami, K.; Itami, K. Catalytic Methods for Aromatic C−H Amination: An Ideal Strategy for Nitrogen-Based Functional Molecules. *ACS Catal.* **2016**, *6*, 610−633. (d) Shaikh, T. M.; Hong, F.-E. Recent developments in the preparation of N-heterocycles using Pd-catalysed C−H activation. *J. Organomet. Chem.* **2016**, *801*, 139−156. (e) Ackermann, L. Carboxylate-Assisted Ruthenium-Catalyzed Alkyne Annulations by C−H/Het−H Bond Functionalizations. *Acc. Chem. Res.* **2014**, *47*, 281−295. (f) Gulevich, A. V.; Dudnik, A. S.; Chernyak, N.; Gevorgyan, V. Transition Metal-Mediated Synthesis of Monocyclic Aromatic Heterocycles. *Chem. Rev.* **2013**, *113*, 3084−3213. (g) Park, J.; Chang, S. Comparative reactivity and selectivity of group 9 Cp*M(III) catalysts in the C−H bond functionalization. *Chem. − Asian J.* **2018**, *13*, 1089−1102.

(3) Gandeepan, P.; Ackermann, L. Transient Directing Groups for Transformative C−H Activation by Synergistic Metal Catalysis. *Chem* **2018**, *4*, 199−222.

(4) (a) Lu, Q.; Greßies, S.; Cembellín, S.; Klauck, F. J. R.; Daniliuc, C. G.; Glorius, F. Redox-Neutral Manganese(I)-Catalyzed C-H Activation: Traceless Directing Group Enabled Regioselective Annulation. *Angew. Chem., Int. Ed.* **2017**, *56*, 12778−12782. (b) Yi, W.; Chen, W.; Liu, F.-X.; Zhong, Y.; Wu, D.; Zhou, Z.; Gao, H. Rh(III)-Catalyzed and Solvent-Controlled Chemoselective Synthesis of Chalcone and Benzofuran Frameworks via Synergistic Dual Directing Groups Enabled Regioselective C−H Functionalization: A Combined Experimental and Computational Study. *ACS Catal.* **2018**, *8*, 9508−9519.

(5) Qian, H.; Huang, D.; Bi, Y.; Yan, G. 2-Propargyl alcohols in Organic Synthesis. *Adv. Synth. Catal.* **2019**, *361*, 3240−3280.

(6) Zhou, X.; Yu, S.; Qi, Z.; Li, X. Rhodium(III)-catalyzed [3+2] annulative coupling between oximes and electron-deficient alkynes. *Sci. China: Chem.* **2015**, *58*, 1297−1301.

(7) (a) Wu, X.; Ji, H. Rhodium-Catalyzed [4 + 1] Cyclization via C−H Activation for the Synthesis of Divergent Heterocycles Bearing a Quaternary Carbon. *J. Org. Chem.* **2018**, *83*, 4650−4656. (b) Wang, F.; Qi, Z.; Sun, J.; Zhang, X.; Li, X. Rh(III)-Catalyzed Coupling of Benzamides with Propargyl Alcohols via Hydroarylation−Lactonization. *Org. Lett.* **2013**, *15*, 6290−6293. (c) Xu, Y.; Wang, F.; Yu, S.; Li, X. Rhodium(III)-catalyzed selective access to isoindolinones via formal [4 + 1] annulation of arylamides and propargyl alcohols. *Chinese J. Catal.* **2017**, *38*, 1390−1398. (d) Wu, X.; Wang, B.; Zhou, S.; Zhou, Y.; Liu, H. Ruthenium-Catalyzed Redox-Neutral [4+1] Annulation of Benzamides and Propargyl Alcohols *via* C-H Bond Activation. *ACS Catal.* **2017**, *7*, 2494−2499. (e) Wu, X.; Wang, B.; Zhou, Y.; Liu, H. Propargyl Alcohols as One-Carbon Synthons: Redox-Neutral Rhodium(III)-Catalyzed C−H Bond Activation for the Synthesis of Isoindolinones Bearing a Quaternary Carbon. *Org. Lett.* **2017**, *19*, 1294−1297.

(8) (a) Hu, X.; Chen, X.; Zhu, Y.; Deng, Y.; Zeng, H.; Jiang, H.; Zeng, W. Rh(III)-Catalyzed Carboamination of PropargylCycloalkanols with Arylamines via Csp^2−H/Csp^3−Csp^3 Activation. *Org. Lett.* **2017**, *19*, 3474−3477. (b) Yan, X.; Ye, R.; Sun, H.; Zhong, J.; Xiang, H.; Zhou, X. Synthesis of 2-Arylindoles by Rhodium-Catalyzed/Copper-Mediated Annulative Coupling of *N*-Aryl-2-aminopyridines and Propargyl Alcohols via Selective C−H/C−C Activation. *Org. Lett.* **2019**, *21*, 7455−7459. (c) Selvaraj, K.; Debnath, S.; Swamy, K. C. K. Reaction of Indole Carboxylic Acid/Amide with Propargyl Alcohols:

[4 + 3]-Annulation, Unexpected 3- to 2- Carboxylate/Amide Migration, and Decarboxylative Cyclization. *Org. Lett.* **2019**, *21*, 5447−5451.

(9) (a) Song, X.; Gao, C.; Li, B.; Zhang, X.; Fan, X. Regioselective Synthesis of 2-Alkenylindoles and 2-Alkenylindole-3-carboxylates through the Cascade Reactions of *N*-Nitrosoanilines with Propargyl Alcohols. *J. Org. Chem.* **2018**, *83*, 8509−8521. (b) Anukumar, A.; Tamizmani, M.; Jeganmohan, M. Ruthenium(II)-Catalyzed Regioselective-Controlled Allenylation/Cyclization of Benzimides with Propargyl Alcohols. *J. Org. Chem.* **2018**, *83*, 8567−8580. (c) Sultana, S.; Shim, J.-J.; Kim, S. H.; Lee, Y. R. Silver(i)/base-promoted propargyl alcohol-controlled regio- or stereoselective synthesis of furan-3-carboxamides and (Z)-enaminones. *Org. Biomol. Chem.* **2018**, *16*, 6749−6759. (d) Nizami, T.; Hua, R. A.; Hua, R. Synthesis of 3H-naphtho[2.1-b]pyran-2-carboxamides from cyclocoupling of β-naphthol, propargyl alcohols and isocyanide in the presence of Lewis acids. *Tetrahedron* **2018**, *74*, 3776−3780.

(10) Gong, W.; Zhou, Z.; Shi, J.; Wu, B.; Huang, B.; Yi, W. Catalyst-Controlled [3 + 2] and [4 + 2] Annulations of Oximes with Propargyl Alcohols: Divergent Access to Indenamines and Isoquinolines. *Org. Lett.* **2018**, *20*, 182−185.

(11) Beletskaya, I. P.; Nájera, C.; Yus, M. Chemodivergent reactions. *Chem. Soc. Rev.* **2020**, *49*, 7101−7166.

(12) (a) Carr, K. J. T.; Davies, D. L.; Macgregor, S. A.; Singh, K.; Villa-Marcos, B. Metal control of selectivity in acetate-assisted C−H bond activation: an experimental and computational study of heterocyclic, vinylic and phenylic C(sp^2)−H bonds at Ir and Rh. *Chem. Sci.* **2014**, *5*, 2340−2346. (b) Chiou, M.-F.; Jayakumar, J.; Cheng, C.-H.; Chuang, S.-C. Impact of the Valence Charge of Transition Metals on the Cobaltand Rhodium-Catalyzed Synthesis of Indenamines, Indenols, and Isoquinolinium Salts: A Catalytic Cycle Involving M^{III}/M^{V} [M = Co, Rh] for [4 + 2] Annulation. *J. Org. Chem.* **2018**, *83*, 7814−7824. (c) Li, J.; Hu, W.; Peng, Y.; Zhang, Y.; Li, J.; Zheng, W. Theoretical Study on Iridacycle and Rhodacycle Formation via C−H Activation of Phenyl Imines. *Organometallics* **2014**, *33*, 2150−2159. (d) Tian, R.; Li, Y.; Liang, C. Mechanism of Rhodium(III)-Catalyzed C−H Activation/Annulation of Aromatic Amide with α-Allenol: A Computational Study. *J. Org. Chem.* **2019**, *84*, 2642−2651. (e) Wang, N.; Li, B.; Song, H.; Xu, S.; Wang, B. Investigation and Comparison of the Mechanistic Steps in the $[(Cp^*MCl_2)_2]$ ($Cp^*=C_5Me_5$; M=Rh, Ir)-Catalyzed Oxidative Annulation of Isoquinolones with Alkynes. *Chem. − Eur. J.* **2013**, *19*, 358−364. (f) Zhao, C.; Ge, Q.; Wang, B.; Xu, X. Comparative investigation of the reactivities between catalysts $[Cp^*RhCl_2]_2$ and $[Cp^*IrCl_2]_2$ in the oxidative annulation of isoquinolones with alkynes: a combined experimental and computational study. *Org. Chem. Front.* **2017**, *4*, 2327−2335. (g) Chen, J.; Guo, W.; Xia, Y. Computational Revisit to the β-Carbon Elimination Step in Rh(III)Catalyzed C−H Activation/Cycloaddition Reactions of *N*-Phenoxyacetamide and Cyclopropenes. *J. Org. Chem.* **2016**, *81*, 2635−2638. (h) Guo, W.; Xia, Y. Mechanistic Understanding of the Divergent Reactivity of Cyclopropenes in Rh(III)-Catalyzed C−H Activation/Cycloaddition Reactions of *N*-Phenoxyacetamide and *N*-Pivaloxybenzamide. *J. Org. Chem.* **2015**, *80*, 8113−8121. (i) Xu, L.; Zhu, Q.; Huang, G.; Cheng, B.; Xia, Y. Computational Elucidation of the Internal Oxidant-Controlled Reaction Pathways in Rh(III)-Catalyzed Aromatic C−H Functionalization. *J. Org. Chem.* **2012**, *77*, 3017−3024. (j) Yang, Y.-F.; Houk, K. N.; Wu, Y.-D. Computational Exploration of Rh^{III}/Rh^{V} and Rh^{III}/Rh^{I} Catalysis in Rhodium(III)-Catalyzed C−H Activation Reactions of *N*-Phenoxyacetamides with Alkynes. *J. Am. Chem. Soc.* **2016**, *138*, 6861−6868. (k) Wang, X.; Gensch, T.; Lerchen, A.; Daniliuc, C. G.; Glorius, F. Cp*Rh(III)/Bicyclic Olefin Cocatalyzed C−H Bond Amidation by Intramolecular Amide Transfer. *J. Am. Chem. Soc.* **2017**, *139*, 6506−6512. (l) Li, J.; Qiu, Z. DFT Studies on the Mechanism of the Rhodium(III)-Catalyzed C−H Activation of *N*-Phenoxyacetamide. *J. Org. Chem.* **2015**, *80*, 10686−10693. (m) Wu, J.-Q.; Zhang, S.-S.; Gao, H.; Qi, Z.; Zhou, C.-J.; Ji, W.-W.; Liu, Y.; Chen, Y.; Li, Q.; Li, X.; Wang, H. Experimental and Theoretical Studies on Rhodium-Catalyzed Coupling of Benzamides with 2,2-Difluorovinyl Tosylate: Diverse Synthesis of Fluorinated Heterocycles. *J. Am. Chem. Soc.* **2017**, *139*, 3537−3545. (n) Melcher, M. C.; von Wachenfeldt, H.; Sundin, A.; Strand, D. Iridium Catalyzed Carbocyclizations: Efficient (5+2) Cycloadditions of Vinylcyclopropanes and Alkynes. *Chem. − Eur. J.* **2015**, *21*, 531−535.

(13) (a) Jiang, J.; Liu, H.; Cao, L.; Zhao, C.; Liu, Y.; Ackermann, L.; Ke, Z. Metallalkenyl, Metallacyclopropene, or Metallallylcarbenoid? RuCatalyzed Annulation between Benzoic Acid and Alkyne. *ACS Catal.* **2019**, *9*, 9387−9392. (b) Lian, B.; Zhang, L.; Fang, D.-C. A computational study on ruthenium-catalyzed [4 + 1] annulation *via* C−H activation: the origin of selectivity and the role of the internal oxidizing group. *Org. Chem. Front.* **2019**, *6*, 2600−2606. (c) Ling, B.; Liu, Y.; Jiang, Y.-Y.; Liu, P.; Bi, S. Mechanistic Insights into the Ruthenium-Catalyzed [4 + 1] Annulation of Benzamides and Propargyl Alcohols by DFT Studies. *Organometallics* **2019**, *38*, 1877−1886. (d) Pei, G.; Liu, Y.; Chen, G.; Yuan, X.; Jiang, Y.-Y.; Bi, S. Unveiling the mechanisms and secrets of chemoselectivities in Au(i)-catalyzed diazo-based couplings with aryl unsaturated aliphatic alcohols. *Catal. Sci. Technol.* **2018**, *8*, 4450−4462. (e) Yu, Y.; Luo, G.; Yang, J.; Luo, Y. Theoretical studies on the N−X (X = Cl, O) bond activation mechanism in catalytic C−H amination. *Catal. Sci. Technol.* **2020**, *10*, 1914−1924. (f) Wu, Y.; Chen, Z.; Yang, Y.; Zhu, W.; Zhou, B. Rh(III)-Catalyzed Redox-Neutral Unsymmetrical C−H Alkylation and Amidation Reactions of *N*-Phenoxyacetamides. *J. Am. Chem. Soc.* **2018**, *140*, 42−45. (g) Duan, P.; Yang, Y.; Ben, R.; Yan, Y.; Dai, L.; Hong, M.; Wu, Y.-D.; Wang, D.; Zhang, X.; Zhao, J. Palladium-catalyzed benzo[d]isoxazole synthesis by C−H activation/[4 + 1] annulation. *Chem. Sci.* **2014**, *5*, 1574−1578. (h) Liu, S.; Pu, M.; Wu, Y.-D.; Zhang, X. computational study on the fate of oxidative directing groups in Ru(II), Rh(III), and Pd(II) catalyzed C-H functionalization. *J. Org. Chem.* **2020**, *85*, 12594−12602. (i) Park, Y.; Heo, J.; Baik, M.-H.; Chang, S. Why is the Ir(III)-Mediated Amido Transfer Much Faster Than the Rh(III)-Mediated Reaction? - A Combined Experimental and Computational Study. *J. Am. Chem. Soc.* **2016**, *138*, 14020−14029. (j) Yu, Y.; Luo, G.; Yang, J.; Luo, Y. Cobalt-CatalysedUnactivated C(sp^3)-H Amination: Two-State Reactivity and Multi-reference Electronic Character. *Catal. Sci. Technol.* **2019**, *9*, 1879−1890. (k) Zhou, X.; Luo, Y.; Kong, L.; Xu, Y.; Zheng, G.; Lan, Y.; Li, X. Cp^*Co^{III}-Catalyzed Branch-Selective Hydroarylation of Alkynes via C−H Activation: Efficient Access to α-*gem*-Vinylindoles. *ACS Catal.* **2017**, *7*, 7296−7304. (l) Li, Y.; Chen, H.; Qu, L.-B.; Houk, K. N.; Lan, Y. Origin of Regiochemical Control in Rh(III)/Rh(V)-Catalyzed Reactions of Unsaturated Oximes and Alkenes to Form Pyrdines. *ACS Catal.* **2019**, *9*, 7154−7165.

(14) Vásquez-Céspedes, S.; Wang, X.; Glorius, F. Plausible Rh(V) Intermediates in Catalytic C−H Activation Reactions. *ACS Catal.* **2018**, *8*, 242−257.

(15) Zheng, G.; Zhou, Z.; Zhu, G.; Zhai, S.; Xu, H.; Duan, X.; Yi, W.; Li, X. Rhodium(III)-Catalyzed Enantio- and DiastereoselectiveC-H Cyclopropylation of N-Phenoxylsulfonamides:Combined Experimental and Computational Studies. *Angew. Chem., Int. Ed.* **2020**, *59*, 2890−2896.

(16) Yang, J.; Wu, L.; Xu, H.; Gao, H.; Zhou, Z.; Yi, W. Redox-Neutral [4 + 2] Annulation of N-Methoxybenzamides with Alkynes Enabled by an Osmium(II)/HOAc Catalytic System. *Org. Lett.* **2019**, *21*, 9904−9908.

(17) Frisch, M. J.; Trucks, G. W.; Schlegel, H. B.; Scuseria, G. E.; Robb, M. A.; Cheeseman, J. R.; Scalmani, G.; Barone, V.; Mennucci, B.; Petersson, G. A.; Nakatsuji, H.; Caricato, M.; Li, X.; Hratchian, H. P.; Izmaylov, J.; Bloino, G.; Zheng, J. L.; Sonnenberg, M.; Hada, M.; Ehara, K.; Toyota, R.; Fukuda, J.; Hasegawa, M.; Ishida, A. F.; Nakajima, T.; Honda, Y.; Kitao, O.; Nakai, H.; Vreven, T.; Montgomery, J. A., Jr.; Peralta, J. E.; Ogliaro, F.; Bearpark, M.; Heyd, J. J.; Brothers, E.; Kudin, K. N.; Staroverov, V. N.; Keith, T.; Kobayashi, R.; Normand, J.; Raghavachari, K.; Rendell, A.; Burant, J. C.; Iyengar, S. S.; Tomasi, J.; Cossi, M.; Rega, N.; Millam, J. M.; Klene, M.; Knox, J. E.; Cross, J. B.; Bakken, V.; Adamo, C.; Jaramillo, J.; Gomperts, R.; Stratmann, R. E.; Yazyev, O.; Austin, A. J.; Cammi, R.; Pomelli, C.; Ochterski, J. W.; Martin, R. L.; Morokuma, K.;

https://doi.org/10.1021/acsomega.1c02183
ACS Omega 2021, 6, 17642−17650

Zakrzewski, V. G.; Voth, G. A.; Salvador, P.; Dannenberg, J. J.; Dapprich, S.; Daniels, A. D.; Farkas, O.; Foresman, J. B.; Ortiz, J. V.; Cioslowski, J.; Fox, D. J. *Gaussian 09*; Revision E.01, Gaussian, Inc.: Wallingford CT, 2013.

(18) (a) Lee, C.; Yang, W.; Parr, R. G. Development of the Colle-Salvetti correlation-energy formula into a functional of the electron density. *Phys. Rev. B* **1988**, *37*, 785−789. (b) Becke, A. D. Density-Functional Thermochemistry. III. The Role of Exact Exchange. *J. Chem. Phys.* **1993**, *98*, 5648−5652.

(19) (a) Wadt, W. R.; Hay, P. J. *Ab initio* effective core potentials for molecular calculations. Potentials for main group elements Na to Bi. *J. Chem. Phys.* **1985**, *82*, 284−298. (b) Hay, P. J.; Wadt, W. R. *Ab initio* effective core potentials for molecular calculations. Potentials for K to Au including the outermost core orbitals. *J. Chem. Phys.* **1985**, *82*, 299−310.

(20) (a) Gonzalez, C.; Schlegel, H. B. An improved algorithm for reaction path following. *J. Chem. Phys.* **1989**, *90*, 2154−2161. (b) Gonzalez, C.; Schlegel, H. B. Reaction path following in mass-weighted internal coordinates. *J. Phys. Chem.* **1990**, *94*, 5523−5527.

(21) Marenich, A. V.; Cramer, C. J.; Truhlar, D. G. Universal solvation model based on solute electron density and on a continuum model of the solvent defined by the bulk dielectric constant and atomic surface tensions. *J. Phys. Chem. B* **2009**, *113*, 6378−6396.

(22) Grimme, S.; Antony, J.; Ehrlich, S.; Krieg, H. A consistent and accurate ab initio parametrization of density functional dispersion correction (DFT-D) for the 94 elements H-Pu. *J. Chem. Phys.* **2010**, *132*, 154104.

(23) Andrae, D.; Häußermann, U.; Dolg, M.; Stoll, H.; Preuß, H. Energy-adjusted *ab initio* pseudopotentials for the second and third row transition elements. *Theoret. Chim. Acta* **1990**, *77*, 123−141.

https://doi.org/10.1021/acsomega.1c02183
ACS Omega 2021, 6, 17642−17650